

Antioxidant Graphene Oxide Nanoribbon as a Novel Whitening Agent Inhibits Microphthalmia-Associated Transcription Factor-Related Melanogenesis Mechanism

Hsin-Yu Chou, Hui-Min David Wang,* Chia-Heng Kuo, Pei-Hsuan Lu, Lin Wang, Wenyi Kang, and Chia-Liang Sun*



Cite This: *ACS Omega* 2020, 5, 6588–6597



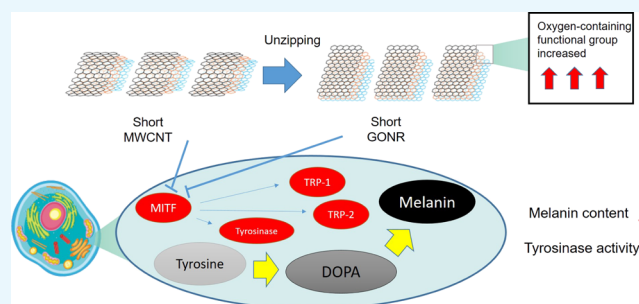
Read Online

ACCESS |

Metrics & More

Article Recommendations

ABSTRACT: In the melanin synthesis process, oxidative reactions play an essential role, and it is a good strategy to inhibit melanin production by reducing oxidative stress. Fullerene and its derivatives, or the complexes, were considered as strong free-radical scavengers, and we further applied multilayered sp^2 nanocarbons to discover melanin synthesis inhibitory mechanisms. In the present study, we used novel nanomaterials, such as multilayered carbon nanotubes (MWCNTs), short-type MWCNTs, graphene oxide nanoribbons (GONRs), and short-type GONRs, as anti-oxidative agents to regulate melanin production. The results showed that GONRs had better anti-oxidative capabilities in intracellular and extracellular oxidative stress analysis platforms than others. We proposed that GONRs have oxygen-containing functional groups. In the 2',7'-dichlorodihydrofluorescein diacetate assay, we found out GONR could chelate metal ions to scavenge reactive oxygen species. In the molecular insight view, we observed that these nanomaterials downregulated the melanin synthesis by decreasing microphthalmia-associated transcription factor-related gene expressions, and there were similar consequences in protein expressions. To sum up, GONRs is a potential agent as a novel antioxidant and skin-whitening cosmetology material.



1. INTRODUCTION

Skin is the organ that covers the outer surface of a human body. Since the interface is in contact with the environment, the skin layer plays an important role in protecting the body against pathogens, avoiding excessive water loss, regulating body temperature, and so on. Melanocytes grow in the basal membrane of the skin epidermis and account for 5% to 10% of the cellular content. They have been characterized as unicellular “glands” having thin, long, streamer-like dendrites and branching. Melanocytes move through the epidermal cells in their immediate vicinity, creating a constellation of epidermal cells around each melanocyte. There are many internal and external causes to skin aging, and one such factor is ultraviolet (UV) radiation from sunlight.¹ During UV exposure, the reactive oxygen species (ROS) levels in the skin increase dramatically, which is known as oxidative stress. Several environmental toxicity factors also enhance oxidative stress to the skin, such as pesticides, carbon tetrachloride, heavy metals, aromatic amines, and particulate matter 2.5 (PM_{2.5}).² In the biochemical mechanism, the intracellular oxidants are generated from the non-enzymatic system, transforming them into ROS to trigger the melanogenesis pathway.³

In addition to ROS, there are many factors that affect melanin production, including gene expression, inflammation, endocrine changes, and pigment uptake.¹ In the first steps of melanin production, tyrosinase plays a role in catalyzing tyrosine into phenomelanin and eumelanin. Both pigments' manufacturing mechanisms are similar, which include L-tyrosine hydroxylation to 3,4-dihydroxy-L-phenylalanine (L-DOPA) and L-DOPA oxidation to dopaquinone. In the next step, dopamine is oxidized by tyrosinase-related protein 1 (TRP-1) and tyrosinase-related protein 2 (TRP-2) in melanosome, which are regulated by the microphthalmia-associated transcription factor (MITF) to form melanin. Finally, melanin is matured and precipitated within the stratum corneum.^{4,5} These penetrate the neighboring keratinocytes of the basal layer and protect their DNA from any UV-induced mutations or modifications. The matured melanin within

Received: December 16, 2019

Accepted: March 9, 2020

Published: March 19, 2020



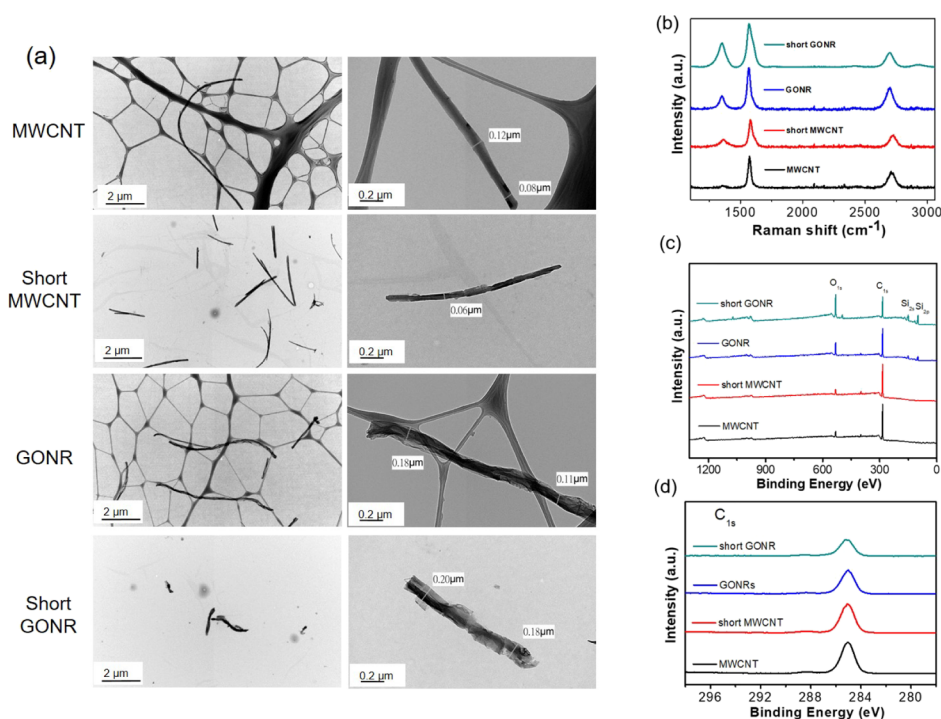


Figure 1. (a) Low-magnification and high-magnification TEM picture of MWCNTs and GONRs. (b) Raman spectra of four nanocarbons. The D band of GONRs is higher than that of MWCNTs after the unzipping process. (c,d) display the X-ray photoelectron spectroscopy spectra of four nanocarbons. Apparently, the D' peak is the most evident for short GONRs.

melanosomes is transferred to keratinocytes^{6–9} and finally leads to a long-lasting pigmentation. Lentigines, freckles, and brown/black spots cause social problems in men and women sometimes. Blocking the oxidative stress or suppressing the tyrosinase activity is one strategy to downregulate the syndrome of hyper-pigmentation and dermatological disorders. Antioxidants heal ROS-caused hyper-pigmentations and cellular damages.^{10,11} Therefore, synthesized anti-oxidative compounds have many biofunctional applications in skin care applications.

Fullerene (C_{60}), carbon nanotube (CNT), graphene, and graphene nanoribbon (GNR) are four kinds of sp^2 nanocarbon widely researched around the world.¹² Fullerene and its derivatives or complexes have been considered strong free-radical scavengers for a long time. Yodoh et al. used water-soluble C_{60} as a protective agent against catabolic stress-induced degeneration. Injac et al. concluded that $C_{60}(OH)_{24}$ is a strong antioxidant compound when the oxidative stress is too high. Okuda et al. suggested that C_{60} complexes can prevent NO-mediated cell injury.^{13,14} Tong et al. showed that C_{60} complexes might be promising candidates for treating brain-related diseases caused by increased levels of superoxide. Actually, a Japanese company identified fullerenes with a strong antioxidant activity for cosmetic use in 2006. Lucente-Schultz et al. demonstrated that the oxygen radical scavenging ability of functionalized single-walled CNTs (SWCNTs) is nearly 40 times greater than that of dendritic C_{60} .^{15–19} Fenoglio et al. observed that multiwalled CNTs (MWCNTs) possess a remarkable radical scavenging capacity in contact with an external source of hydroxyl or superoxide radical.²⁰ Density functional theory calculations also revealed a model of SWCNTs as free-radical scavengers. In 2004, Novoselov et al. first demonstrated that graphene exhibited a strong ambipolar electric effect and could be promising for electronic

applications.²¹ Following that, they continued to show that graphene has electronic properties that are distinctive for a 2D gas of particles described by the Dirac equation.^{22,23} Since these two groundbreaking papers, more and more attention has been given to the graphene-based research.^{24–30} For example, Qiu et al. in 2014 showed that graphene oxide and few-layer graphene exhibit a significant antioxidant activity and can protect various biomolecular molecules from oxidation.³¹ Han et al. experimentally demonstrated in 2007 that the energy gap of GNRs can be controlled during the lithography process by changing the ribbon width.³² Among the four nanocarbons, GNRs have received the least attention. To our knowledge, there is little research on the antioxidant properties of graphene oxide nanoribbons (GONRs).^{31,33} Hence, in this study, we carefully prepared MWCNTs, short MWCNTs, GONRs, and short GONRs and aimed to compare their antioxidant properties and related results systematically.

2. RESULTS AND DISCUSSION

2.1. Morphology of MWCNTs and GONRs. Figure 1a shows the low- and high-magnification transmission electron microscopy (TEM) images of MWCNTs and short MWCNTs. Following acidic cutting under ultrasonication, the length of MWCNTs could be shortened from $>10 \mu\text{m}$ to $2\text{--}3 \mu\text{m}$. Simultaneously, it was observed that the nitric acid treatment roughens the smooth tube surfaces. Some notches and irregular shapes are displayed in the high-magnification picture. Further, using MWCNTs and short MWCNTs through microwave reactions obtains GONR and short GONR, respectively. We also illustrated the low- and high-magnification TEM pictures of GONR and short GONR. Owing to the major longitudinal unzipping and minor horizontal cutting, it seems that GONRs were shorter than MWCNTs. On the other hand, high-magnification pictures

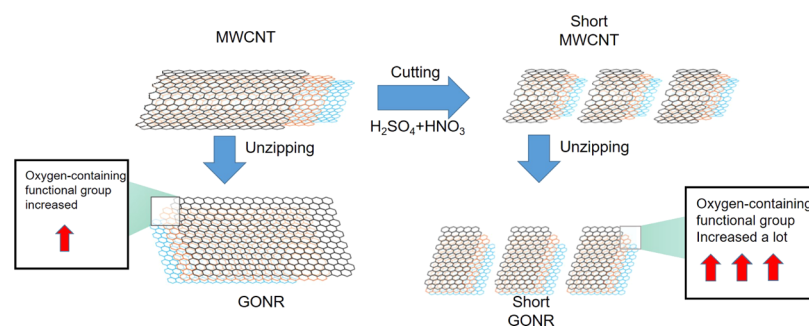


Figure 2. Process diagram of unzipping and cutting presented MWCNTs to be GONRs and short GONRs.

showed larger diameters, that is, 0.11–0.18 μm , of GONRs than those of MWCNTs, indicating that the unzipping process was successful. Similarly, short GONRs exhibited a shorter length and larger diameter than short MWCNTs. In the air compressor of our new unzipping process, the thin layered structures of the GONRs were less than what we obtained in the early report for the same microwave power of 250 W while maintaining the thicker central MWCNTs.¹² This meant a core–shell MWCNT/GONR heterostructure would more likely appear instead of the fully unzipped nanoribbon structure through all microwave powers in the new process. To compare with the short GONR in our previous studies,³⁴ the higher microwave power generated more notches on the side of the ribbons and did not form nice, smooth ribbon edges. Note that we used two different kinds of Cu grids in Figure 1a. For MWCNTs and GONRs with enough length, the Gu grid with a lacey formvar stabilized with carbon (product no. 01881-F, Ted Pella, Inc., USA) was utilized. The open holes in a lacey carbon film prevented an overlapping transmission image between nanocarbons and the carbon film. The dark gray networks belong to the lacey carbon film. However, the Gu grid with formvar stabilized with carbon (product no. 01800-F, Ted Pella, Inc., USA) was needed for short MWCNT and short GONR. This was because the big holes in the lacey carbon film caused problems for holding the short MWCNT and short GONR efficiently. As illustrated in Figure 1, the light gray contrast beneath the short MWCNTs and short GONRs is a light layer of carbon. This carbon layer stabilized the formvar film exposed to the electron beam via its heat- and electrical-conducting properties.

2.2. Bonding Configurations of MWCNTs and GONRs.

The Raman spectra of the four nanocarbons are presented in Figure 1b; the D band of GONRs was higher than that of MWCNTs after the unzipping process. This was attributed to the higher oxidation level and greater number of edge structures of GONR compared to MWCNTs. This phenomenon is also similar to what we observed in 2011.¹² Owing to the high graphitization level, the G band of MWCNTs had the lowest full-width-at-half-maximum number. The I_D/I_G ratios of the four nanocarbons were 0.076, 0.502, 0.483, and 0.700, respectively. Briefly, the decreased length and surface oxidation increased the defect level and thus made the I_D/I_G ratios higher. The D' peak is present in all defective graphenes and is viewed as a measure of quality.³⁵ As illustrated in Figure 1b, the D' peaks in the four spectra become more prominent after either the cutting or unzipping process, suggesting that they are destructive processes that introduce many defects. Figure 1c,d display the X-ray photoelectron spectroscopy spectra of the four nanocarbons. Apparently, the D' peak is the clearest for

short GONRs. As shown in Figure 1c, the O level significantly increased from 7.6% (MWCNTs) to 19.9% (GONRs) due to the strong oxidation ability of KMnO_4 in an acidic environment. On the other hand, the O level slightly increased by 0.8% from MWCNT to the short MWCNTs. Importantly, the highest O level is 38.3% for the short GONR, implying that the ends of the nanoribbons would be easier to attach oxygen functional groups than the planar sp^2 surfaces. The larger full-width-at-half-maximum number and the shift to a high binding energy of C 1s peaks after the unzipping process of both MWCNTs and short MWCNTs are illustrated in Figure 1d. For graphene oxides, the deconvoluted peaks in the high-binding-energy side could be assigned to C–C(C=C), C–O, C=O, and COOH bondings.³⁶ We characterized GONR (200 W) in 2013,³⁷ and the results were similar to this study results. This study concluded the phenomena of Raman spectra, meaning that more oxygen-containing functional groups were generated during the tube-to-ribbon transformation (Figure 2).

2.3. Anti-oxidative Properties of MWCNTs and GONRs.

2.3.1. Determination of 1,1-Diphenyl-2-picrylhydrazyl Free Radical Scavenging Activity Assays. 1,1-Diphenyl-2-picrylhydrazyl (DPPH) free-radical scavenging activity is an antioxidant platform applied to detect the anti-oxidative capacity; the results for the four nanocarbons are described in Table 2. In the DPPH assay, vitamin C at a concentration of 100 μM was used as a positive control. To test the anti-oxidative activities of MWCNTs, short MWCNTs, GONRs, and short GONRs, dosages of 1, 5, and 10 mg/L were incubated into the reaction solution to measure the properties. MWCNTs, short MWCNTs, GONRs, and short

Table 1. Nucleotide Sequences of Primers Were Used in This Study

	MITF
forward:	5'-TTGGTGCCACCTAAACATTGT-3'
reverse:	5'-CCGTTGGCCTTGCTGTATG-3'
	Tyrosinase
forward:	5'-CTGCCAACGATCCTATCTTCCT-3'
reverse:	5'-GGTTATGTCCAATGGGTGCATT-3'
	TRP-1
forward:	5'-GGTTTATTTGACACGCCTCCTT-3'
reverse:	5'-AGACTTCGAACAGCAGGGTCAT-3'
	TRP-2
forward:	5'-GCACACATGTAACCTCTGTG-3'
reverse:	5'-TCA TAT AAG CAG GCT TGG CC-3'
	GADPH
forward:	5'-GCACCACCACTGCTTAGCA-3'
reverse:	5'-TCTTCTGGGTGGCAGTGATG-3'

Table 2. Antioxidant Activities of Nanocarbons, Including Reducing Power, DPPH Free-Radical Scavenging Activity, and Ferrous Ion-Chelating Power^a

	concentration (mg/L)	DPPH (%)	chelating (%)	reducing power (OD ₇₀₀)
vitamin C	100 μ M	93.4 \pm 0.1		
EDTA	100 μ M		90.4 \pm 0.0	
BHA	100 μ M			1.86 \pm 0.05
MWCNT	1	9.6 \pm 0.5	13.8 \pm 0.2	0.99 \pm 0.06
	5	17.3 \pm 1.0	21.4 \pm 0.5	1.04 \pm 0.07
	10	19.2 \pm 0.3	29.2 \pm 0.8	1.11 \pm 0.04
short MWCNT	1	5.4 \pm 0.4	11.5 \pm 0.2	1.09 \pm 0.00
	5	8.8 \pm 0.1	22.4 \pm 0.3	1.11 \pm 0.00
	10	12.1 \pm 0.3	28.7 \pm 0.7	1.13 \pm 0.03
GONR	1	5.0 \pm 1.0	33.8 \pm 0.2	1.02 \pm 0.07
	5	15.2 \pm 0.2	41.4 \pm 0.5	1.13 \pm 0.00
	10	26.8 \pm 0.3	69.7 \pm 0.6	1.15 \pm 0.01
short GONR	1	5.2 \pm 1.0	35.5 \pm 0.3	1.07 \pm 0.06
	5	16.8 \pm 0.6	43.2 \pm 0.1	1.15 \pm 0.02
	10	30.0 \pm 0.4	68.9 \pm 0.3	1.11 \pm 0.00

^aAll data points were done in triplicates.

GONRs had moderate inhibitory abilities at 10 mg/L (19.2 \pm 0.3, 12.1 \pm 0.3, 26.8 \pm 0.3, and 30.0 \pm 0.4%), while vitamin C had a similar condition at 100 μ M (93.4 \pm 0.1%) for the suppression.

2.3.2. Ion-Chelating Activity Assay. Within the oxidative stress situation, the ferrozine can develop a complex with Fe²⁺ to be measured quantitatively. In the presence of chelating mediators, the complex is broken, causing the ferrous ions to reduce from a dark red color of the Fe²⁺ complex. We used EDTA as the positive control. Table 2 shows that MWCNTs, short MWCNTs, GONRs, and short GONRs had chelating activity at 10 mg/L (29.2 \pm 0.8, 28.7 \pm 0.7, 69.7 \pm 0.6, and 68.9 \pm 0.3%), while the positive control had the similar condition at 100 μ M (93.4 \pm 0.1%).

2.3.3. Ferric-Reducing Antioxidant Power Measurement. The ferric-reducing potential assay is a simple and reliable test used to quantify the Fe(III)–ferricyanide complex synthesis. In this assay, the reducing power of the four nanocarbons

producing the ferrous Fe(III)–TPTZ complex was detected by changes in the color of the solution from yellow to green and blue. Table 2 demonstrates that the reducing powers of MWCNT, short MWCNT, GONR, and short GONR were optical density (OD) 1.11, 1.13, 1.15, and 1.11 at 10 mg/L.

2.3.4. MWCNTs and GONRs Inhibit Intracellular ROS Accumulation. Many reports have shown that ROS destroys the structural integrity of cell membranes, including cell membranes and nuclear membranes to lead to cell damage and to loss of normal function.^{38–40} In addition, ROS is also one of the important factors to catalyze tyrosinase forming melanin, and the inhibition of ROS production is a good strategy to downregulate melanin synthesis. In this study, we used the 2',7'-dichlorodihydrofluorescein diacetate (DCFDA) staining assay to analyze the intracellular oxidative stress level in MWCNT and GONR treatment cells. Phorbol 12-myristate 13-acetate (PMA) induced oxidative stimulations in MWCNT and GONR groups and was used as a negative control.⁴¹ When the concentration of PMA was 20 ng/mL, it induced oxidative stress, increasing the value to 38%; after treating GONRs and MWCNTs, the levels of ROS were downregulated to the normal level. The data showed that both materials inhibited oxidative stress levels, and the anti-oxidative effect of GONRs was higher than that of MWCNTs (Figure 3). Table 1 shows a similar consequence list. We contended that there are three reasons for our new findings: first, the order of solubility of these materials was as follows: short GONRs > GONRs > short MWCNTs > MWCNTs, meaning that the contact area of short GONRs was the largest, so it was superior for ROS scavenging. Second, GONRs and MWCNTs were sp²-carbon structures that could destroy ROS electricity through adduct formation or electron transfer.⁴² We found that the antioxidant effects of the nanoribbon structures were better than those of the nanotube structures, so nanoribbons make it easier to transfer electrons than nanotubes. Finally, in Figure 1b, we observe that the GONR sp²-carbon site contained more oxygen functional groups than MWCNTs, the carboxylic acid groups could chelate metal ions, and the hydroxyl groups could be a H-donor to scavenge ROS and inhibit melanin production.

2.4. Cytotoxicity of MWCNTs and GONRs Treated in Human Dermal Fibroblast Cells. The 3-(4,5-Dimethylth-

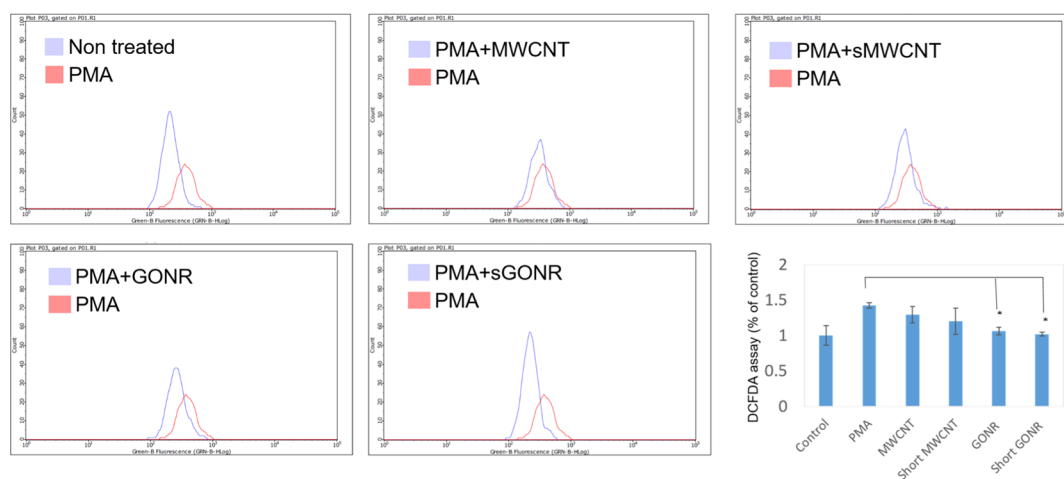


Figure 3. DCFDA assay results showing that MWCNTs and GONRs treatment decreased the ROS production in B16 F10 cells. All data points were done in triplicates (**P* < 0.01; Student's *t*-test).

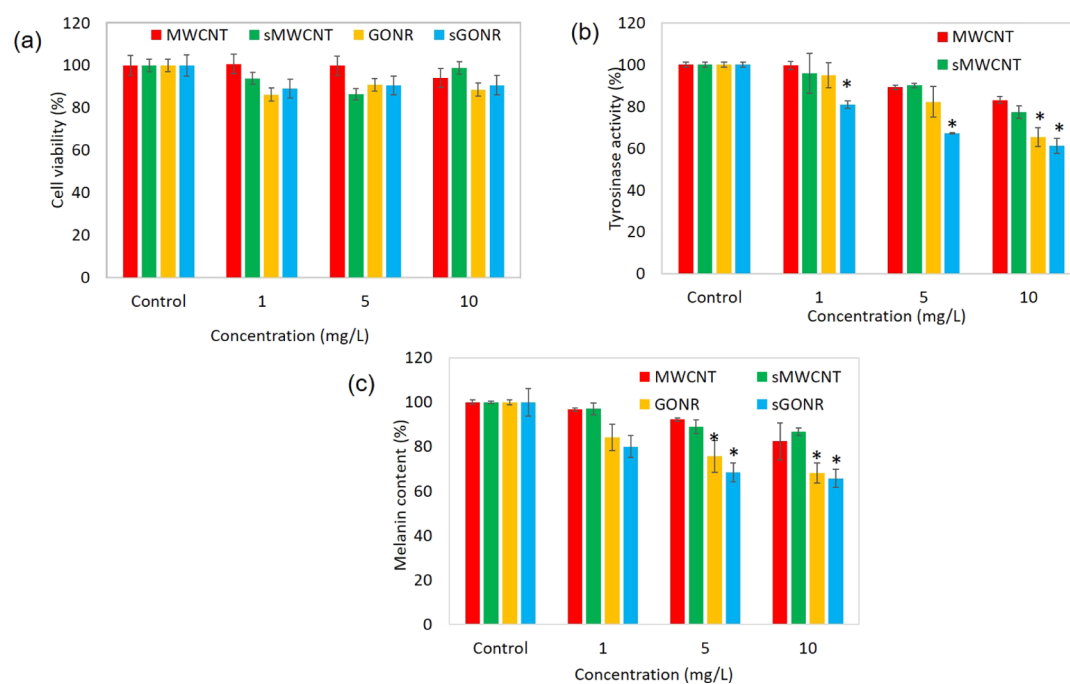


Figure 4. (a) Cell proliferation effects of nanoparticles on human cells. HS68 cells were treated with 1, 5, and 10 $\mu\text{g}/\text{mL}$ of MWCNTs and GONRs for 24 h. (b) Tyrosinase activity assay. B16–F10 cells were treated with 1, 5, and 10 $\mu\text{g}/\text{mL}$ of MWCNTs and GONRs. (c) Inhibitory effects of melanin content of nanocarbons on B16–F10 cells. All data points were done in triplicates ($*P < 0.01$; Student's *t*-test).

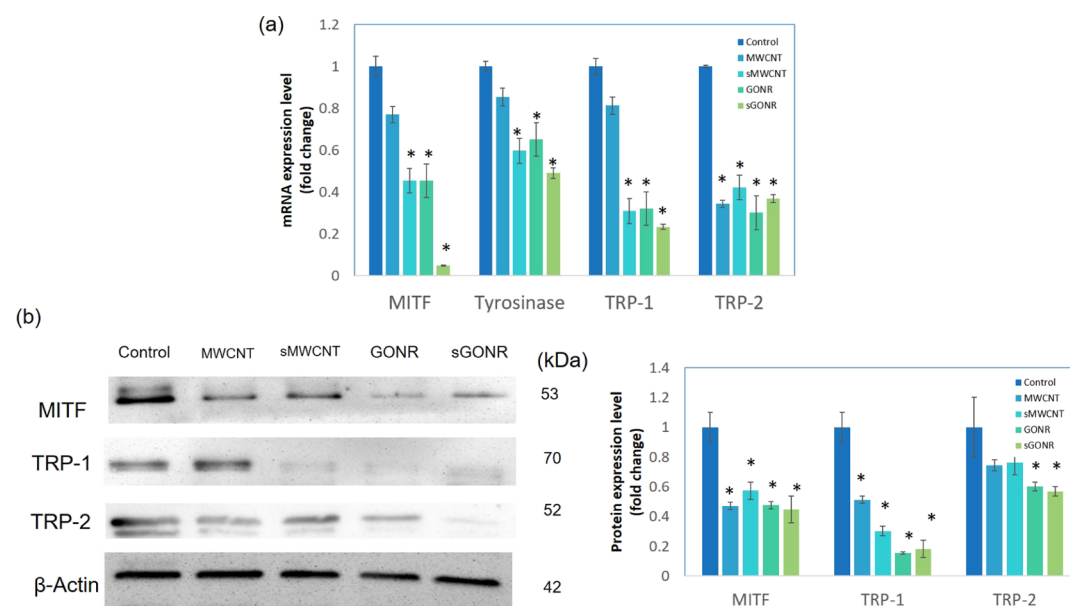


Figure 5. RNA and protein expressions associated with the melanin biosynthesis of B16 F10 cells treated with various concentrations (0, 15, and 10 $\mu\text{g}/\text{mL}$) of MWCNTs and GONRs. (a) RNA expressions. (b) Protein expressions. All data points were done in triplicates ($*P < 0.01$; Student's *t*-test).

iazol-2-yl)-2,5-diphenyltetrazolium bromide (MTT) method was applied to evaluate the cytotoxic properties of GONRs on Hs68 cells (Figure 3), and cells were cultured at different doses of 1, 5, and 10 $\mu\text{g}/\text{mL}$. We examined that the cell viabilities of MWCNT were 100.7 ± 3.7 , 99.8 ± 4.9 , and $94.1 \pm 4.7\%$ at concentrations of 1, 5, and 10 $\mu\text{g}/\text{mL}$, respectively; viabilities for the short MWCNT were calculated in the same order and were found to be 93.9 ± 2.2 , 86.4 ± 3.0 , and $98.9 \pm 2.1\%$. We observed that the B16–F10 cells were incubated in high concentrations, and the cell survival of Hs68 cells was more than 80%, suggesting that the MWCNT and short MWCNT

had no toxic effect on human dermal fibroblasts cells. The cell viabilities of GONR and short GONR were 86.24 ± 2.1 , 90.87 ± 3.5 , 88.58 ± 2.5 , 89.03 ± 3.6 , 90.71 ± 2.8 , and $90.64 \pm 2.5\%$. It is also pointed out in Figure 4a that GONR and short GONR did not have a discernible cytotoxic effect on HS68 cells. In previous reports, the use of untested nanomaterials for cosmetic purposes could be considered questionable,^{43,44} and it was usually due to the attack of DNA after the nanoparticles entered the cells. After cytotoxicity test, we found that our materials did not cause toxicity to normal skin cells. We concluded that after nanomaterials entered the cells, the

nanomaterials just inhibit melanin production by decreasing the oxidative stress and chelating metal ions and do not damage the mitochondria or DNA, which means that MWCNTs and GONRs were safe to be used.

2.5. Two Types of MWCNTs and GONRs in B16–F10 Cellular Tyrosinase Activity and Melanin Content. In the melanin synthesis pathway, tyrosinase plays a critical role. Tyrosinase oxidizes and forms eumelanin and pheomelanin through a series of biochemical reactions. In order to determine whether GONRs and MWCNTs inhibit the activities of tyrosinase and cause a decrease in melanin production, we analyzed the tyrosinase activity in B16–F10 cells. We found that MWCNTs and short MWCNTs inhibited the tyrosinase activity by approximately 17.1% and 23% at 10 mg/L. GONRs and short GONRs had better effect in suppressing the tyrosinase activity at the same concentrations compared to another GONR. They were also in a dose-dependent manner and inhibited 49.8% and 44.7% of the tyrosinase activity, as shown in Figure 4b.

Melanin is an indispensable pigment in the human body, but the overexpression of melanin often triggers a series of diseases. In previous studies, Xiao et al. used a similar material, Radical Sponge, a fullerene nanoparticle, as an anti-melanin agent.⁴⁵ There were some good results; about 20% of melanin production could be inhibited. In order to improve its efficiency, we further improved the testing material to measure the inhibition rate of melanin and its molecular mechanism, as shown in Figures 4c and 5. MWCNTs and short MWCNTs decreased the melanin content by 17.6 ± 5.5 and $13.2 \pm 0.2\%$ at 10 mg/L and in a dose-dependent manner. GONRs and short GONRs powerfully downregulated the values to 32.0 ± 2.3 and $35.3 \pm 3.4\%$ at 10 mg/L. The experimental results suggested that all four types could inhibit the synthesis of melanin and GONRs had a stronger effect. On the other hand, we have also observed that the short GONR has a better effect in inhibiting the melanin production. We conclude that the short GONRs has more functional groups and can effectively prevent metal ions-catalyzed tyrosinase, further inhibiting the production of melanin (Figure 2). In Table 1, we observe that the effort of metal ion-chelating short type is higher than the normal type; this means that these short GONRs could be potentially applied in the cosmetic field as skin care agents.

2.6. Mechanism of MWCNTs and GONRs Inhibited the B16–F10 Cellular Melanin Content. Cells respond to the external oxidative stress by regulating the protein expression. B16–F10 cells enhance *c-myc* gene expression and up-regulated AMPK to decrease oxidative levels,⁴⁶ and in this work, MITF is a specific transcription factor of tyrosinase to regulate the molecular melanin synthesis signal pathway.^{47–49} In Figure 5a, MWCNTs and GONRs downregulate the microphthalmia-associated transcription factor by reducing the oxidative stress, and then, downstream gene TRP-1 and TRP-2 were also downregulated. For the protein level, a similar phenomenon was found, whereby MWCNTs and GONRs downregulated the MITF-related melanogenesis pathway and then finally reduced the melanin content (Figure 5b).

3. EXPERIMENTAL MATERIALS AND METHODS

3.1. Preparation of MWCNTs and GONRs. The relevant process for making GONRs was reported in a previous paper.¹² MWCNT (0.05 g) was suspended in 9:1 H₂SO₄/H₃PO₄ and treated with a microwave reactor (CEM-Discover) with the power set at 250 W for 2 min. After the addition of KMnO₄

(0.25 g) to the solutions, the solutions were treated with the same microwave power at 65 °C for 4 min.¹² We then modified this process using a shorter second-stage microwave time of 8 min by utilizing an air compressor. Here, the air compressor is used to control the temperature of the microwave reactor during the process. The microwave power was set at 250 W in the preliminary tests.

3.2. Preparation of Short MWCNTs and Short GONRs. The relevant process for making short GONRs was reported in our previous paper.³⁴ The acidic treatment time was chosen as 8 h. The microwave power was set at 250 W, which is the same as that for getting GONRs.

3.3. DPPH Radical Scavenging Activity. DPPH was frequently used to decide the scavenging capacity of samples and the antioxidation properties.⁵⁰ DPPH is a purple reagent that changes the color from purple to yellow if the free radical is transferred to the analyte. Positive anti-oxidative samples with suitable concentrations were added to the solution, and the samples were analyzed at 517 nm for 30 min. We used the percentages of the remaining DPPH besides the testing samples to measure the amount of antioxidant required to reduce the previous DPPH radicals. Vitamin C at 100 μM was used as the positive control. The scavenging activity (%) was measured as

$$\text{Scavenging capacity (\%)} = \frac{(A_{\text{sample}} - A_{\text{blank}})}{(A_{\text{control}} - A_{\text{blank}})} \times 100\% \quad (1)$$

3.4. Metal-Chelating Activity. Metal ion is the factor that causes lipid excessive oxidation, and Fe²⁺ is one of the most influencing ions.⁵⁰ Different concentrations of nanobiomaterial (1 μL) were loaded into a 96-well plate, which contained 2 mM FeCl₂·4H₂O (10 μL), and then loaded into ferrozine (5 mM, 20 μL). The admixture was fully blended with 69 μL menthol and kept at room temperature for 10 min. Then, the sample reaction solution was observed at 562 nm. EDTA was used as a positive control at 100 μM, and the metal-chelating activity calculation formula was based on eq 1.

3.5. Reducing Power. The calculation of reducing power is based on a previous study.⁵⁰ First, 2.5 μL graphene materials was mixed with PBS buffer (67 mM, pH 6.8) and K₃Fe(CN)₆ (2.5 μL, 20%) and then incubated at 50 °C for 20 min. Then, 10% trichloro acetic acid (160 μL) was blended with the reagents at 300g centrifuged for 20 min. The absorption length was determined at 700 nm after being mixed with 25 μL FeCl₃ (2%). Butylated hydroxyanisole (BHA) was used at 100 μM.

3.6. Cell Proliferation Examinations. The human dermal fibroblasts cell line HS68 was employed to analyze the ratio of cell proliferation. HS68 was incubated in Dulbecco's modified Eagle medium (DMEM) containing 10% fetal bovine serum and 1% penicillin and streptomycin mixed.^{50,51} After being treated with different concentrations of samples, we applied MTT to detect the cell proliferation ratio. 8000 cells were seeded in 96-well plates and treated with samples for 24 h. The supernatant solution was removed, and we used the MTT solution to culture for 2 h at 37 °C. After incubation, we removed the MTT-containing media and dissolved it with dimethyl sulfoxide (DMSO). The solution was read at OD 590 nm and the rate calculated by eq 1.

3.7. Assessment of Cellular Melanin Contents. We used a method with minor modifications based on the previous assay.^{52,53} Cell pellets of B16–F10 from Bioresource

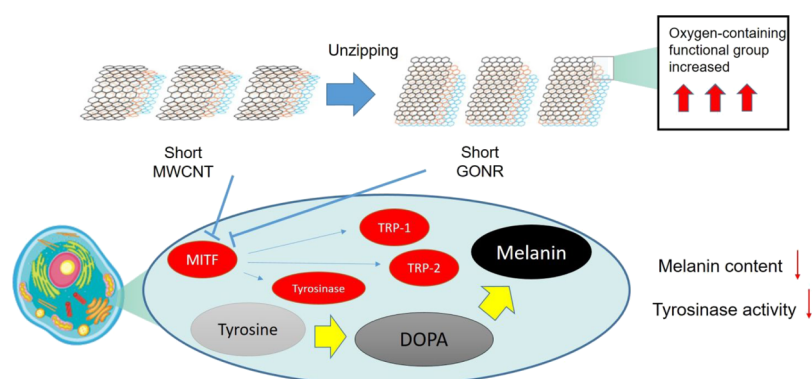


Figure 6. Schematic diagram of biofunctions of MWCNTs and GONRs in B16 F10 cells. MWCNTs and GONRs could inhibit melanin synthesis via redox oxidation and regulating MITF related pathway.

Collection and Research Center (BCRC, CRL 6323, Hsinchu, Taiwan) were dissolved in a mixture of 2.0 N NaOH and 10% DMSO. The sample was subsequently heated for 1 h at 90 °C and centrifuged at 10,000g for another 10 min to obtain the clarified supernatant. The melanin count was determined by monitoring the OD of the supernatant at 475 nm.

3.8. B16–F10 Cellular Tyrosinase Activity. For the B16–F10 cellular tyrosinase activity, we referred to the previous work with some modifications.⁵⁰ Cells were cultured in 12-well plates at 10^5 cells each well. After treatments with samples, cells were lysed in 1% Triton X-100/PBS and 2 mM L-tyrosine (50 μ L) for 3 h. After the incubation, we removed the media and read the absorbance at OD 590 nm. The tyrosinase activity formula was computed by eq 1.

3.9. Detection of ROS by DCFDA Staining. Referring to the previous study,⁵⁴ 1.2×10^5 B16–F10 cells were seeded in 6-well plates and treated with various concentrations of samples. Cells were suspended in PBS and then loaded with DCFDA (5 μ M) in non-phenol red DMEM for 30 min at 37 °C. The flow cytometer (Guava, Merck, Germany) was used to detect the fluorescent signal of DCFDA. Excitation and emission wavelengths of DCFDA were 488 and 535 nm, respectively.

3.10. Quantitative Real-Time Polymerase Chain Reaction. We followed the methods of Lin et al. (2018).¹ Real-time quantitative reverse transcription polymerase chain reaction (qRT-PCR) consisted an exclusive primer probe to generate fluorescence. It used a fluorescence detection technique that senses each cycle using a 7500 qRT-PCR System (Applied Biosystems, USA). It detected the cycle based on the amount of fluorescence released, and then the product of each cycle was calculated for the generated content, which resulted in achieving real-time quantitative purposes. Trizol (Invitrogen, USA) was used to extract a complete RNA of the lung tissue, as per the direction given by the manufacturer. Subsequently, a reverse transcription kit (Takara, Japan) was used to generate DNA. In the qRT-PCR using primers, listed in Table 1, first, the sample was heated to form a single strand of DNA; then a primer binding took place to form a double-stranded DNA (dsDNA), after which SYBR Green dsDNA was combined, for which the SYBR green plus reagent kit (Roche, Basel, Swiss) was used, which resulted in releasing fluorescence. The resultant was passed through a fluorescence detection system. The detection of fluorescent signals took place during the elongation or annealing phase of each cycle; after the detection, the sample contents were back-pushed by

the detected fluorescence intensities.⁵⁵ The expression levels of target genes were normalized to α -tubulin levels using the $2^{-\Delta\Delta C_t}$ method.

3.11. Western Blot Test. B16–F10 cells were lysed at 4 °C overnight with a radioimmunoprecipitation assay buffer (Thermo Scientific Co., USA), which contains protease inhibitors. The bicinchoninic acid protein assay kit (BCA, Sigma-Aldrich Corp., USA) was used to quantify the protein amount. Sample proteins were separated on 10% sodium dodecyl sulfate-polyacrylamide gel and transferred on to a polyvinylidene difluoride (PVDF) membrane (PALL Life Science, Ann Arbor, MI, USA). The PVDF membrane was blocked with a blocking buffer (Thermo Scientific) for 1 h and incubated with the specific primary antibody overnight at 4 °C. Next, the membrane was washed with Tris buffered saline-Tween 20 buffer twice and incubated with secondary antibodies for 1.5 h. After that, the membrane was dipped into chemiluminescence detection reagents (Thermo Scientific) and analyzed by a MiniChemi Chemiluminescence imager (Beijing Sage Creation Science, China). Sources of antibodies included rabbit anti-MITF, rabbit anti-TRP-1, rabbit anti-TRP-2, and β -actin (Thermo Scientific).

3.12. Material Analysis. TEM (JEOL JEM-1230, 100 kV) was utilized to observe the morphology of the nanocarbons. A micro Raman spectrometer (PTT, RAMaker) was applied to check the resonance modes of the nanocarbons. X-ray photoelectron spectroscopy (XPS, Kratos Axis Ultra DLD) measurements were also carried out for determining the compositional analysis.^{12,34}


3.13. Statistical Analysis. All the samples and standard experiments were repeated at least three times. We applied the Student's *t*-test to compare and express the average of the mean values \pm standard deviation statistically.

4. CONCLUSIONS

To sum up, we observed that the short GONR was a potential material for skin care production due to its multiple biofunctional properties (Figure 6). The results showed that the nanocarbons played a role as an extracellular and intracellular antioxidant. Meanwhile, the nanocarbon inhibited the tyrosinase activity and the melanin content and did not cause any serious injury to pigment cells. This work established the anti-melanogenesis functions of four types of nanocarbons; future studies will be examined about the mechanism of these compounds on specific gene and protein expressions related to melanin maturation, transportation, and accumulation.

■ AUTHOR INFORMATION

Corresponding Authors

Hui-Min David Wang – Ph.D. Program in Tissue Engineering and Regenerative Medicine and Graduate Institute of Biomedical Engineering, National Chung Hsing University, Taichung City 402, Taiwan; Graduate Institute of Medicine, College of Medicine, Kaohsiung Medical University, Kaohsiung City 807, Taiwan; Department of Medical Laboratory Science and Biotechnology, China Medical University, Taichung City 404, Taiwan; College of Food and Biological Engineering, Jimei University, Xiamen 361021, PR China;  orcid.org/0000-0002-4692-4917; Phone: 886-935753718; Email: davidw@dragon.nchu.edu.tw; Fax: 886-4-22852242; <https://sites.google.com/site/davidbiocosme/home>

Chia-Liang Sun – Department of Chemical and Materials Engineering, Chang Gung University, Taoyuan City 333, Taiwan; Department of Neurosurgery, Linkou Chang Gung Memorial Hospital, Taoyuan City 333, Taiwan; Phone: 886-3-2118800 ext. 5379; Email: sunchialiang@gmail.com; Fax: 886-3-2118668; <http://www.suncl.idv.tw/>

Authors

Hsin-Yu Chou – Ph.D. Program in Tissue Engineering and Regenerative Medicine, National Chung Hsing University, Taichung City 402, Taiwan

Chia-Heng Kuo – Department of Chemical and Materials Engineering, Chang Gung University, Taoyuan City 333, Taiwan

Pei-Hsuan Lu – Department of Dermatology, Linkou Chang Gung Memorial Hospital, Taoyuan City 333, Taiwan; Taipei Arts Plastic Clinic, Taipei 106, Taiwan

Lin Wang – College of Chemistry & Pharmacy, Northwest A&F University, Yangling, Shaanxi 712100, PR China

Wenyi Kang – Joint International Research Laboratory of Food & Medicine Resource Function, Henan University, Kaifeng 475004, Henan Province, PR China

Complete contact information is available at:
<https://pubs.acs.org/10.1021/acsomega.9b04316>

Author Contributions

H.-Y.C. and H.-M.D.W. contributed equally to this work. H.-M.D.W., H.-Y.C., and C.-L.S. conceived and designed the experiments; H.-Y.C., C.-H.K., P.-H.L., and L.W. performed the experiments and analyzed the data; C.-L.S., W.K., and H.-M.D.W. contributed the reagents, materials, and analysis tools; H.-Y.C., C.-L.S., and H.-M.D.W. wrote the article.

Notes

The authors declare no competing financial interest.
The data used to support the findings of this study are available from the corresponding author upon request.

■ ACKNOWLEDGMENTS

This work was supported by grants from the Ministry of Science and Technology (MOST 108-2221-E-005-044) and Chang Gung Memorial Hospital (BMRPA64 and CMRPD2F0041); we thank the projects of the Research Center for Sustainable Energy and Nanotechnology, NCHU 107S0203B. H.-Y.C. carried out his thesis research under the auspices of the PhD Program in Tissue Engineering and Regenerative Medicine, National Chung Hsing University and National Health Research Institutes.

■ REFERENCES

- (1) Lin, L.-C.; Chen, C.-Y.; Kuo, C.-H.; Lin, Y.-S.; Hwang, B. H.; Wang, T. K.; Kuo, Y.-H.; Wang, H.-M. D. 36H: A Novel Potent Inhibitor for Antimelanogenesis. *Oxid. Med. Cell. Longevity* **2018**, *2018*, 6354972.
- (2) Li, R.; Qiu, X.; Xu, F.; Lin, Y.; Fang, Y.; Zhu, T. Macrophage-Mediated Effects of Airborne Fine Particulate Matter (PM_{2.5}) on Hepatocyte Insulin Resistance in Vitro. *ACS Omega* **2016**, *1*, 736–743.
- (3) You, Y.-J.; Wu, P.-Y.; Liu, Y.-J.; Hou, C.-W.; Wu, C.-S.; Wen, K.-C.; Lin, C.-Y.; Chiang, H.-M. Sesamol Inhibited Ultraviolet Radiation-Induced Hyperpigmentation and Damage in C57BL/6 Mouse Skin. *Antioxidants* **2019**, *8*, 207.
- (4) Hseu, Y.-C.; Cheng, K.-C.; Lin, Y.-C.; Chen, C.-Y.; Chou, H.-Y.; Ma, D.-L.; Leung, C.-H.; Wen, Z.-H.; Wang, H.-M. Synergistic Effects of Linderanolid B Combined with Arbutin, PTU or Kojic Acid on Tyrosinase Inhibition. *Curr. Pharm. Biotechnol.* **2015**, *16*, 1120–1126.
- (5) Bae-Harboe, Y.-S. C.; Park, H.-Y. Tyrosinase: a central regulatory protein for cutaneous pigmentation. *J. Invest. Dermatol.* **2012**, *132*, 2678–2680.
- (6) Rezapour-Lactoe, A.; Yeganeh, H.; Ostad, S. N.; Gharibi, R.; Mazaheri, Z.; Ai, J. Thermoresponsive polyurethane/siloxane membrane for wound dressing and cell sheet transplantation: In vitro and in vivo studies. *Mater. Sci. Eng., C* **2016**, *69*, 804–814.
- (7) Boo, Y. C. p-Coumaric Acid as An Active Ingredient in Cosmetics: A Review Focusing on its Antimelanogenic Effects. *Antioxidants* **2019**, *8*, 275.
- (8) Awan, F.; Islam, M. S.; Ma, Y.; Yang, C.; Shi, Z.; Berry, R. M.; Tam, K. C. Cellulose Nanocrystal-ZnO Nanohybrids for Controlling Photocatalytic Activity and UV Protection in Cosmetic Formulation. *ACS Omega* **2018**, *3*, 12403–12411.
- (9) Cristina Negritto, M.; Valdez, C.; Sharma, J.; Rosenberg, C.; Selassie, C. R. Growth Inhibition and DNA Damage Induced by X-Phenols in Yeast: A Quantitative Structure-Activity Relationship Study. *ACS Omega* **2017**, *2*, 8568–8579.
- (10) Hamelian, M.; Hemmati, S.; Varmira, K.; Veisi, H. Green synthesis, antibacterial, antioxidant and cytotoxic effect of gold nanoparticles using Pistacia Atlantica extract. *J. Taiwan Inst. Chem. Eng.* **2018**, *93*, 21–30.
- (11) Meneses-Gutiérrez, C. L.; Hernández-Damián, J.; Pedraza-Chaverri, J.; Guerrero-Legarreta, I.; Téllez, D. L.; Jaramillo-Flores, M. E. Antioxidant Capacity and Cytotoxic Effects of Catechins and Resveratrol Oligomers Produced by Enzymatic Oxidation against T24 Human Urinary Bladder Cancer Cells. *Antioxidants* **2019**, *8*, 214.
- (12) Sun, C.-L.; Chang, C.-T.; Lee, H.-H.; Zhou, J.; Wang, J.; Sham, T.-K.; Pong, W.-F. Microwave-assisted synthesis of a core-shell MWCNT/GONR heterostructure for the electrochemical detection of ascorbic acid, dopamine, and uric acid. *ACS Nano* **2011**, *5*, 7788–7795.
- (13) Lin, T.-E.; Lu, Y.-J.; Sun, C.-L.; Pick, H.; Chen, J.-P.; Lesch, A.; Girault, H. H. Soft Electrochemical Probes for Mapping the Distribution of Biomarkers and Injected Nanomaterials in Animal and Human Tissues. *Angew. Chem., Int. Ed. Engl.* **2017**, *56*, 16498–16502.
- (14) Okuda, K.; Hirota, T.; Hirobe, M.; Nagano, T.; Mochizuki, M.; Mashino, T. Synthesis of various water-soluble G60 derivatives and their superoxide-quenching activity. *Fullerene Sci. Technol.* **2000**, *8*, 127–142.
- (15) Lucente-Schultz, R. M.; Moore, V. C.; Leonard, A. D.; Price, B. K.; Kosynkin, D. V.; Lu, M.; Partha, R.; Conyers, J. L.; Tour, J. M. Antioxidant single-walled carbon nanotubes. *J. Am. Chem. Soc.* **2009**, *131*, 3934–3941.
- (16) Injac, R.; Perse, M.; Obermajer, N.; Djordjevic-Milic, V.; Prijatelj, M.; Djordjevic, A.; Cerar, A.; Strukelj, B. Potential hepatoprotective effects of fullereneol C60(OH)₂₄ in doxorubicin-induced hepatotoxicity in rats with mammary carcinomas. *Biomaterials* **2008**, *29*, 3451–3460.
- (17) Tong, J.; Zimmerman, M. C.; Li, S.; Yi, X.; Luxenhofer, R.; Jordan, R.; Kabanov, A. V. Neuronal uptake and intracellular

superoxide scavenging of a fullerene (C60)-poly(2-oxazoline)s nanoformulation. *Biomaterials* **2011**, *32*, 3654–3665.

(18) Yudoh, K.; Shishido, K.; Murayama, H.; Yano, M.; Matsubayashi, K.; Takada, H.; Nakamura, H.; Masuko, K.; Kato, T.; Nishioka, K. Water-soluble C60 fullerene prevents degeneration of articular cartilage in osteoarthritis via down-regulation of chondrocyte catabolic activity and inhibition of cartilage degeneration during disease development. *Arthritis Rheum.* **2007**, *56*, 3307–3318.

(19) Takada, H.; Mimura, H.; Xiao, L.; Islam, R. M.; Matsubayashi, K.; Ito, S.; Miwa, N. Innovative Anti-Oxidant: Fullerene (INCI #: 7587) is as “Radical Sponge” on the Skin. Its High Level of Safety, Stability and Potential as Premier Anti-Aging and Whitening Cosmetic Ingredient. *Fullerenes, Nanotubes, Carbon Nanostruct.* **2006**, *14*, 335–341.

(20) Fenoglio, I.; Greco, G.; Tomatis, M.; Muller, J.; Raymundo-Piñero, E.; Béguin, F.; Fonseca, A.; Nagy, J. B.; Lison, D.; Fubini, B. Structural defects play a major role in the acute lung toxicity of multiwall carbon nanotubes: physicochemical aspects. *Chem. Res. Toxicol.* **2008**, *21*, 1690–1697.

(21) Novoselov, K. S.; Geim, A. K.; Morozov, S. V.; Jiang, D.; Zhang, Y.; Dubonos, S. V.; Grigorieva, I. V.; Firsov, A. A. Electric field effect in atomically thin carbon films. *Science* **2004**, *306*, 666–669.

(22) Novoselov, K. S.; Geim, A. K.; Morozov, S. V.; Jiang, D.; Katsnelson, M. I.; Grigorieva, I. V.; Dubonos, S. V.; Firsov, A. A. Two-dimensional gas of massless Dirac fermions in graphene. *Nature* **2005**, *438*, 197–200.

(23) Zhou, X.; Wei, Y.; He, Q.; Boey, F.; Zhang, Q.; Zhang, H. Reduced graphene oxide films used as matrix of MALDI-TOF-MS for detection of octachlorodibenzo-p-dioxin. *Chem. Commun.* **2010**, *46*, 6974–6976.

(24) Zhao, W.; Fan, S.; Xiao, N.; Liu, D.; Tay, Y. Y.; Yu, C.; Sim, D.; Hng, H. H.; Zhang, Q.; Boey, F.; Ma, X.; Zhang, H.; Yan, Q. Flexible carbon nanotube papers with improved thermoelectric properties. *Energy Environ. Sci.* **2012**, *5*, 5364–5369.

(25) Wang, Z.; Wu, S.; Zhang, J.; Chen, P.; Yang, G.; Zhou, X.; Zhang, Q.; Yan, Q.; Zhang, H. Comparative studies on single-layer reduced graphene oxide films obtained by electrochemical reduction and hydrazine vapor reduction. *Nanoscale Res. Lett.* **2012**, *7*, 161.

(26) Liang, X.; Fu, Z.; Chou, S. Y. Graphene transistors fabricated via transfer-printing in device active-areas on large wafer. *Nano Lett.* **2007**, *7*, 3840–3844.

(27) Sun, X.; Liu, Z.; Welsher, K.; Robinson, J. T.; Goodwin, A.; Zaric, S.; Dai, H. Nano-graphene oxide for cellular imaging and drug delivery. *Nano Res.* **2008**, *1*, 203–212.

(28) Chen, W.; Xiao, P.; Chen, H.; Zhang, H.; Zhang, Q.; Chen, Y. Polymeric Graphene Bulk Materials with a 3D Cross-Linked Monolithic Graphene Network. *Adv. Mater.* **2019**, *31*, 1802403.

(29) Chen, D.; Feng, H.; Li, J. Graphene oxide: preparation, functionalization, and electrochemical applications. *Chem. Rev.* **2012**, *112*, 6027–6053.

(30) Ranjan, P.; Agrawal, S.; Sinha, A.; Rao, T. R.; Balakrishnan, J.; Thakur, A. D. A Low-Cost Non-explosive Synthesis of Graphene Oxide for Scalable Applications. *Sci. Rep.* **2018**, *8*, 12007.

(31) Qiu, Y.; Wang, Z.; Owens, A. C. E.; Kulaots, I.; Chen, Y.; Kane, A. B.; Hurt, R. H. Antioxidant chemistry of graphene-based materials and its role in oxidation protection technology. *Nanoscale* **2014**, *6*, 11744–11755.

(32) Han, M. Y.; Ozyilmaz, B.; Zhang, Y.; Kim, P. Energy band-gap engineering of graphene nanoribbons. *Phys. Rev. Lett.* **2007**, *98*, 206805.

(33) Souza, J. P.; Mansano, A. S.; Venturini, F. P.; Santos, F.; Zucolotto, V. Antioxidant metabolism of zebrafish after sub-lethal exposure to graphene oxide and recovery. *Fish Physiol. Biochem.* **2019**, *45*, 1289–1297.

(34) Sun, C.-L.; Su, C.-H.; Wu, J.-J. Synthesis of short graphene oxide nanoribbons for improved biomarker detection of Parkinson's disease. *Biosens. Bioelectron.* **2015**, *67*, 327–333.

(35) King, A. A. K.; Davies, B. R.; Noorbehesht, N.; Newman, P.; Church, T. L.; Harris, A. T.; Razal, J. M.; Minett, A. I. A New Raman

Metric for the Characterisation of Graphene oxide and its Derivatives. *Sci. Rep.* **2016**, *6*, 19491.

(36) Hsu, H.-C.; Shown, I.; Wei, H.-Y.; Chang, Y.-C.; Du, H.-Y.; Lin, Y.-G.; Tseng, C.-A.; Wang, C.-H.; Chen, L.-C.; Lin, Y.-C.; Chen, K.-H. Graphene oxide as a promising photocatalyst for CO₂ to methanol conversion. *Nanoscale* **2013**, *5*, 262–268.

(37) Lin, L.-Y.; Yeh, M.-H.; Tsai, J.-T.; Huang, Y.-H.; Sun, C.-L.; Ho, K.-C. A novel core-shell multi-walled carbon nanotube@graphene oxide nanoribbon heterostructure as a potential supercapacitor material. *J. Mater. Chem. A* **2013**, *1*, 11237–11245.

(38) Yin, H.; Xu, L.; Porter, N. A. Free radical lipid peroxidation: mechanisms and analysis. *Chem. Rev.* **2011**, *111*, 5944–5972.

(39) Tung, C.-H.; Chang, J.-H.; Hsieh, Y.-H.; Hsu, J.-C.; Ellis, A. V.; Liu, W.-C.; Yan, R.-H. Comparison of hydroxyl radical yields between photo- and electro-catalyzed water treatments. *J. Taiwan Inst. Chem. Eng.* **2014**, *45*, 1649–1654.

(40) Ohshima, H.; Yoshie, Y.; Auriol, S.; Gilbert, I. Antioxidant and pro-oxidant actions of flavonoids: effects on DNA damage induced by nitric oxide, peroxynitrite and nitroxyl anion. *Free Radical Biol. Med.* **1998**, *25*, 1057–1065.

(41) Chou, H.-Y.; Lee, C.; Pan, J.-L.; Wen, Z.-H.; Huang, S.-H.; Lan, C.-W.; Liu, W.-T.; Hour, T.-C.; Hseu, Y.-C.; Hwang, B.; Cheng, K.-C.; Wang, H.-M. Enriched Astaxanthin Extract from *Haematococcus pluvialis* Augments Growth Factor Secretions to Increase Cell Proliferation and Induces MMP1 Degradation to Enhance Collagen Production in Human Dermal Fibroblasts. *Int. J. Mol. Sci.* **2016**, *17*, 955.

(42) Bitner, B. R.; Marciano, D. C.; Berlin, J. M.; Fabian, R. H.; Cherian, L.; Culver, J. C.; Dickinson, M. E.; Robertson, C. S.; Pautler, R. G.; Kent, T. A.; Tour, J. M. Antioxidant carbon particles improve cerebrovascular dysfunction following traumatic brain injury. *ACS Nano* **2012**, *6*, 8007–8014.

(43) Liao, C.; Li, Y.; Tjong, S. Graphene Nanomaterials: Synthesis, Biocompatibility, and Cytotoxicity. *Int. J. Mol. Sci.* **2018**, *19*, 3564.

(44) Kong, H.; Wang, L.; Zhu, Y.; Huang, Q.; Fan, C. Culture medium-associated physicochemical insights on the cytotoxicity of carbon nanomaterials. *Chem. Res. Toxicol.* **2015**, *28*, 290–295.

(45) Xiao, L.; Matsubayashi, K.; Miwa, N. Inhibitory effect of the water-soluble polymer-wrapped derivative of fullerene on UVA-induced melanogenesis via downregulation of tyrosinase expression in human melanocytes and skin tissues. *Arch. Dermatol. Res.* **2007**, *299*, 245–257.

(46) Kfoury, A.; Armario, M.; Collodet, C.; Sordet-Dessimoz, J.; Giner, M. P.; Christen, S.; Moco, S.; Leleu, M.; Leval, L.; Koch, U.; Trumpp, K.; Sakamoto, K.; Beermann, F.; Radtke, F. AMPK promotes survival of c-Myc-positive melanoma cells by suppressing oxidative stress. *EMBO J.* **2018**, *37*, No. e97673.

(47) Hseu, Y.-C.; Cheng, K.-C.; Lin, Y.-C.; Chen, C.-Y.; Chou, H.-Y.; Ma, D.-L.; Leung, C.-H.; Wen, Z.-H.; Wang, H.-M. Synergistic Effects of Linderanolide B Combined with Arbutin, PTU or Kojic Acid on Tyrosinase Inhibition. *Curr. Pharm. Biotechnol.* **2015**, *16*, 1120–1126.

(48) Lee, S.; Kim, J.; Song, H.; Seok, J.; Hong, S.; Boo, Y. Luteolin 7-Sulfate Attenuates Melanin Synthesis through Inhibition of CREB- and MITF-Mediated Tyrosinase Expression. *Antioxidants* **2019**, *8*, 87.

(49) Duval, C.; Cohen, C.; Chagnoleau, C.; Flouret, V.; Bourreau, E.; Bernerd, F. Key regulatory role of dermal fibroblasts in pigmentation as demonstrated using a reconstructed skin model: impact of photo-aging. *PLoS One* **2014**, *9*, No. e114182.

(50) Li, P.-H.; Chiu, Y.-P.; Shih, C.-C.; Wen, Z.-H.; Ibetto, L. K.; Huang, S.-H.; Chiu, C. C.; Ma, D.-L.; Leung, C.-H.; Chang, Y.-N.; Wang, H.-M. D. Biofunctional Activities of *Equisetum ramosissimum* Extract: Protective Effects against Oxidation, Melanoma, and Melanogenesis. *Oxid. Med. Cell. Longevity* **2016**, *2016*, 2853543.

(51) Liang, C.-H.; Chan, L.-P.; Ding, H.-Y.; So, E. C.; Lin, R.-J.; Wang, H.-M.; Chen, Y.-G.; Chou, T.-H. Free Radical Scavenging Activity of 4-(3,4-Dihydroxybenzoyloxymethyl)phenyl-O-β-d-glucopyranoside from *Origanum vulgare* and Its Protection against Oxidative Damage. *J. Agric. Food Chem.* **2012**, *60*, 7690–7696.

(52) Wang, H.-M.; Chen, C.-Y.; Wen, Z.-H. Identifying melanogenesis inhibitors from *Cinnamomum subavenium* with in vitro and in vivo screening systems by targeting the human tyrosinase. *Exp. Dermatol.* **2011**, *20*, 242–248.

(53) Wang, Y.-C.; Haung, X.-Y.; Chiu, C.-C.; Lin, M.-Y.; Lin, W.-H.; Chang, W.-T.; Tseng, C.-C.; Wang, H.-M. D. Inhibitions of melanogenesis via *Phyllanthus emblica* fruit extract powder in B16F10 cells. *Food Biosci.* **2019**, *28*, 177–182.

(54) Panchuk, R. R.; Skorokhyd, N. R.; Kozak, Y. S.; Lehka, L. V.; Moiseenok, A. G.; Stoika, R. S. Tissue-protective activity of selenomethionine and D-panthetine in B16 melanoma-bearing mice under doxorubicin treatment is not connected with their ROS scavenging potential. *Croat. Med. J.* **2017**, *58*, 171.

(55) Wang, H.-M. D.; Chen, C.-C.; Huynh, P.; Chang, J.-S. Exploring the potential of using algae in cosmetics. *Bioresour. Technol.* **2015**, *184*, 355–362.